


## Properties of packings and dispersions of superellipse sector particles

John Colt,<sup>1</sup> Lucas Nelson<sup>2</sup>, Sykes Cargile<sup>2</sup>, Ted Brzinski<sup>2,\*</sup> and Scott V. Franklin<sup>1</sup>

<sup>1</sup>*School of Physics and Astronomy, Rochester Institute of Technology, Rochester, New York 14623-5603, USA*

<sup>2</sup>*Department of Physics and Astronomy, Haverford College, Haverford, Pennsylvania 19041, USA*

 (Received 14 October 2022; revised 6 December 2023; accepted 18 December 2023; published 9 February 2024)

Superellipse sector particles (SeSPs) are segments of superelliptical curves that form a tunable set of hard-particle shapes for granular and colloidal systems. SeSPs allow for continuous parametrization of corner sharpness, aspect ratio, and particle curvature; rods, circles, rectangles, and staples are examples of shapes SeSPs can model. We compare three computational processes: pair-wise Monte Carlo simulations that explore particle-particle geometric constraints, Monte Carlo simulations that reveal how these geometric constraints play out over dispersions of many particles, and Molecular Dynamics simulations that form random loose and close packings. We investigate the dependence of critical random loose and close packing fractions on particle parameters, finding that both values increase with opening aperture and decrease with increasing corner sharpness. The identified packing fractions are compared with the mean-field prediction of the random contact model; we find deviations from the model's prediction due to correlations between particle orientations. The complex interaction of spatial proximity and orientational alignment is also explored with a generalized spatioorientational distribution area (SODA) plot, which shows how higher density packings are achieved through particles assuming a small number of preferred configurations that depend sensitively on particle shape and system preparation.

DOI: [10.1103/PhysRevE.109.024901](https://doi.org/10.1103/PhysRevE.109.024901)

### I. INTRODUCTION

A striking finding of packings of elongated rods [1,2] or convex particles [3,4] is their entanglement, which can produce bulk cohesion despite the absence of attractive inter-particle potentials. A pile's particle shape-related resistance to tensile forces is called geometric cohesion, and the study of these systems represents a relatively new area of research in the broader field of granular materials. Until recently, there has been no general framework by which to systematically categorize particle shapes or move smoothly from one shape to another to explore how important behaviors arise as a function of particle shape.

Critical granular packing fractions (e.g., random close and random loose packings) depend strongly on the symmetries of the constituent particles [5]. For two-dimensional systems such as the ones studied here, the area packing fraction is defined as the fraction of the total system area occupied by particles,  $\phi = \frac{N_{\text{particle}} A_{\text{particle}}}{A_{\text{system}}}$ , with random close and loose packings the greatest and lowest packing fractions at which disordered packings can form. Particle anisometry can result in an increased angle of repose [6,7], even exceeding 90° [7,8]. Packings of staples, rigid and flexible rods, and star- and z-shaped particles can exhibit tensile strength [9], with relevance for aleatory design [10] and strengthening granular materials under strain [11–13]. Banana-shaped or bent-core rods are of broad interest to the liquid crystal community because of their rich phase space [14–17]. Semicircular particles

are a compelling, quasi-2D model system for the study of homodimerization and chirality-driven phase separation [18,19], and entropy approaches have been applied successfully to colloidal crystals of a variety of shapes [20,21]. Recently, Ref. [22] used Monte Carlo techniques to investigate packings of hard, circular arcs, analytically identifying the densest configurations, which were compared with simulations to identify the likelihood of their appearing in bulk packings.

Reference [23] introduced a new construct, the superellipsoidal sector particle (SeSP), that can model a wide variety of particle shapes, including stars, circles, discorectangles, and staples, by parametrizing the Lamé curve  $|x|^m + |y/A|^n = 1$  as

$$\begin{bmatrix} x(\theta) \\ y(\theta) \end{bmatrix} = \begin{bmatrix} |\cos \theta|^{2/n} A \text{sign}(\cos \theta) \\ |\sin \theta|^{2/m} \text{sign}(\sin \theta) \end{bmatrix}. \quad (1)$$

$A$  is the particle aspect ratio,  $m$  and  $n$  the superellipse degrees which control particle curvature, and the particle is restricted to a segment  $\theta \in [\theta_{\min}, \theta_{\max}]$ . Reference [23] calculated the excluded area for a characteristic set of SeSPs and mapped the complicated relationship between orientation and relative position for nonoverlapping configurations of a pair of SeSPs. Lu *et al.* [24] conducted MD simulations of packings of straight and curved spherocylinders and identified preferred nearest-neighbor configurations with features similar to those seen by Ref. [23] in entangled isolated pair configurations. In this work, we study the relationship between features of the configurations of isolated pairs of SeSPs and the preferred neighbor configurations that emerge in dense dispersions and packings.

\*Corresponding author: [tbrzinski@haverford.edu](mailto:tbrzinski@haverford.edu)

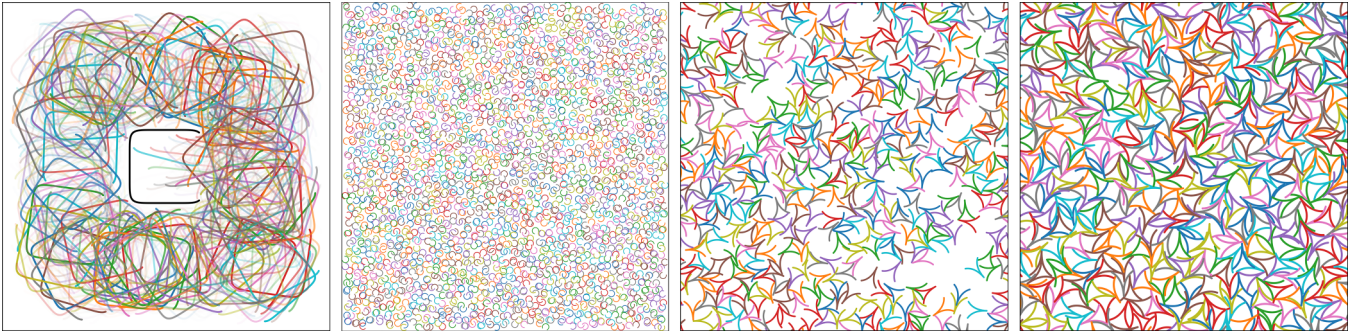


FIG. 1. Left: Sample particle placements from a pairwise Monte Carlo simulation. Center left: A dispersion of  $\sim 3000$  SeSPs created through a Monte Carlo simulation. Center right: A loose packing of 500 SeSPs created through a Molecular Dynamics simulation. Right: A close packing of 500 SeSPs created through a Molecular Dynamics simulation. Different SeSP parameters were chosen to represent the diversity of particle shapes.

## II. METHODOLOGY

The particle-pair metrics introduced in Ref. [23] are based on a straightforward Monte Carlo method (described in more depth in Ref. [1]) which proceeds as follows: (i) a particle is fixed at the origin, (ii) a second particle is placed at a random location and orientation, and, if there is no overlap with the first, the configuration is recorded. The second particle is then moved to a new (random) location and orientation and again checked for overlap.

Dispersions are created with a generalization of the same Monte Carlo (MC) method: Particles are placed one at a time at random locations and orientations in an extended space and checked for overlap with all previously placed particles. If an overlap is present, the newly placed particle is removed. In contrast to the pairwise study, nonoverlapping particles are not removed. Instead, the process repeats with newly located and oriented particles and continues until the desired packing fraction has been reached or no new particles can be placed without overlap (within some long computational time frame). A typical dispersion simulation attempts  $10^6$  particle placements, with resulting dispersions containing  $\mathcal{O}(10^3)$  particles.

In order to extend our study to rigid packings, we use the well-established LAMMPS molecular dynamics (MD) software package [25]. In these simulations, a given number of particles are placed randomly and at low density within a 2D space and slowly expanded. We approximate SeSP particles by placing  $N$  circles (diameter  $d = 0.1$ ) along a superellipse “backbone;” these circles overlap and are held fixed relative to one another and do not otherwise interact with each other. We use an adaptive-stepsize Runge-Kutta algorithm to ensure even spacing, even around sharp corners; the effect on the excluded area and other characteristics is minimal as long as the core “thickness”  $D$  is much smaller than any other length-scales. Particle contact is checked by looking for overlaps between all circles on one particle with all circles on another; particle positions then evolve according to Newton’s Laws, with a repulsive interaction force that scales as  $(\delta r - d)^{3/2}$ , where  $\delta r$  is the separation between the circle center lines. Thus, in contrast with the MC simulations, SeSPs in our MD simulations are effectively soft. Simulations are over-damped to suppress numerical noise; the damping coefficient is such that the particle lengthscale grows by only  $10^{-6}$  in the time it

takes velocities to decay by a factor of  $1/e$ , ensuring that the simulation is effectively quasistatic.

The transition to random loose packing (RLP), the concentration at which the system transitions from a liquid dispersion to a rigid packing, is identified with a rigidity percolation criterion. Rigidity percolation defines the state of the system in terms of particle clusters which are rigid independent of other clusters. We assess internal structure rigidity with a pebble game algorithm [26] in which the contact network is assessed using rules similar to the board games checkers or sternhalma (commonly called “Chinese checkers”) to compare the number of mechanical constraints and degrees of freedom according to the Maxwell counting criteria [27]. The process uses a modified version of software published by Silke Henkes [28], and we identify jamming as the concentration at which the largest rigid cluster spans the system. The scaling of these rigid structures as the system approaches jamming is a well-established metric by which to characterize the state of the system [29–35], allowing us to connect to a broad library of prior research on particulate matter. We continue the quasistatic expansion of the particles until particle intersection is impossible to avoid and identify random close packing (RCP) as the highest density state of a packing without such aphysical configurations. Both RLP and RCP show global randomness, even if local order exists, similar to random packings of discs, which can show local regions of hexagonal packing.

Examples of dispersions and packings prepared by each of the procedures described above are shown in Fig. 1. We note the initial randomness of particle placement in the MD simulations is similar to that in the low-density MC-generated dispersions by construction. The heterogeneity as the system approaches random loose packing evolves as particles come into contact and rearrange as they grow. RLP represents the least-dense, rigid network. Rigidity percolation was achieved in the absence of any noncontact body forces. Thus, the packings are mechanically stable at RLP, but would compact further if subjected to any finite, outside stress, such as a gravitational force. In this work, we investigate SeSPs with aspect ratio  $A = 1$  and equal superellipse degrees  $m = n$ , and choose segments  $[\theta_{\min}, \theta_{\max}]$  such that the opening in the SeSP subtends particular polar angles  $\Psi$  measured relative to the center of curvature and centered on the  $x$  axis.

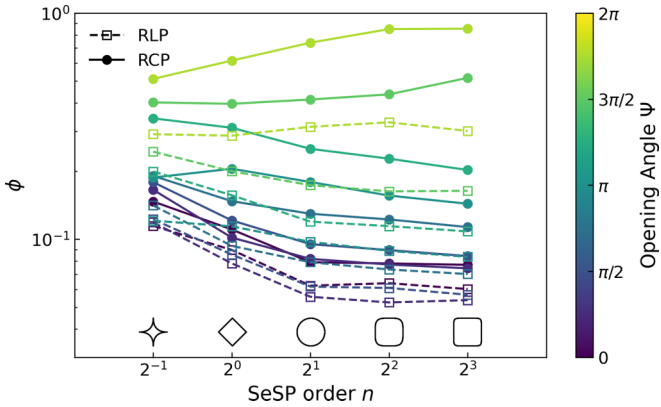


FIG. 2. Critical packing fractions plotted vs SeSP exponent  $n$ , showing the dependence on corner sharpness. Colors indicate the opening angle of the SeSPs, line and marker types indicate whether the packing fraction is measured at random loose or random close packing, and the inset at the bottom shows representative SeSPs of the various orders included with zero opening angle.

III. RESULTS

A. Packing fractions and coordination numbers

The values of the random loose and random close packing fractions for the chosen subset of SeSPs as functions of exponent for different opening apertures  $\Psi$  are shown in Fig. 2. The opening aperture is indicated by color, ranging from dark blue ( $\Psi = 0$ , a closed particle) to light green ( $\Psi \rightarrow 2\pi$ , an almost completely open particle). As expected, the critical packing fractions increase with the opening aperture, as particles with larger openings allow entanglement configurations that result in denser packings. With the exception of only the most open particle shapes, both random loose (open boxes) and random close (closed circles) decrease with corner sharpness (SeSP order  $n$ ). The sharper corners (and correspondingly straight sides) of higher-order SeSPs impose stronger rotational constraints between SeSPs, leading to less dense packings.

The particular case of  $n = 2$  and  $\Psi = 0$  (hollow ring-shaped particles) can be compared with monodisperse circular discs, which reach RCP around  $\phi = 0.88$ . While the empty area enclosed by a ring-shaped particle results in a much lower value of  $\phi_{RCP}$ , our observed critical packing fraction of  $\phi \approx 0.05$  is equivalent to a packing of rigid disks near  $\phi = 0.88$  for  $\langle \delta r \rangle \approx 0.3d$ , consistent with the results of our simulations.

Philipse *et al.* [36] developed a mean-field model, the random contact model, to explain the aspect-ratio dependence of the packing fraction of long, thin sticks. This model posits that critical packing fractions scale inversely with the excluded area  $A_{excl}$ , a purely geometric conclusion from the reasoning that if each particle pair occupies, on average,  $2A_{excl}$ , a packing fraction  $\phi$  implies  $\langle c \rangle = \frac{\phi A_{excl}}{2A_{part}}$  contacts per particle ( $A_{part}$  is the particle area and the factor of two avoids double-counting contacts). This argument is shape independent and rests solely on the definition of the excluded area as the area forbidden to a second particle by the existence of the first and the assumption that there are no positional or orientational correlations

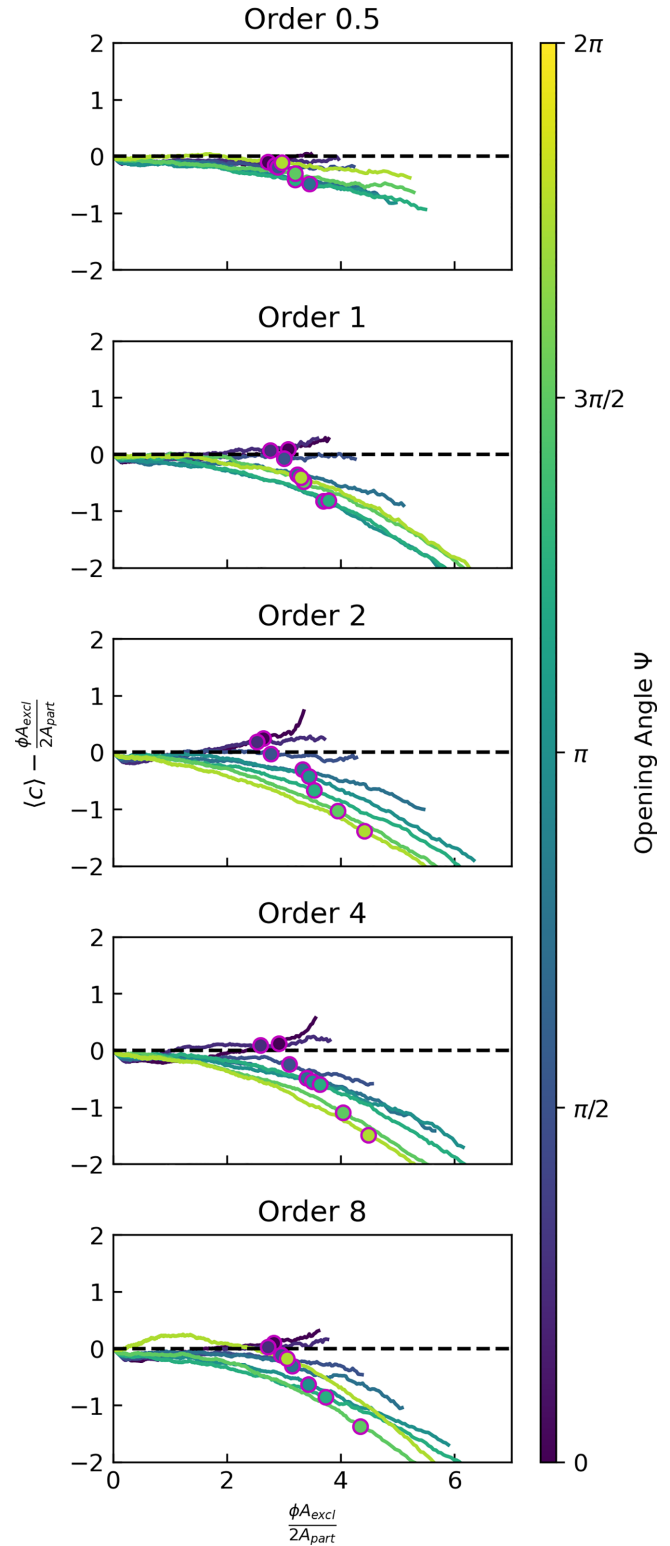


FIG. 3. Mean coordination number minus the product of excluded area and number density plotted against the product of excluded area and number density. Each colored line represents a full molecular dynamics simulation with a different shape of SeSP, terminating at random close packing with a circular marker at random loose packing. For an uncorrelated random dispersion, per the random contact model (RCM), the quantity should equal zero (indicated by a dashed black line).

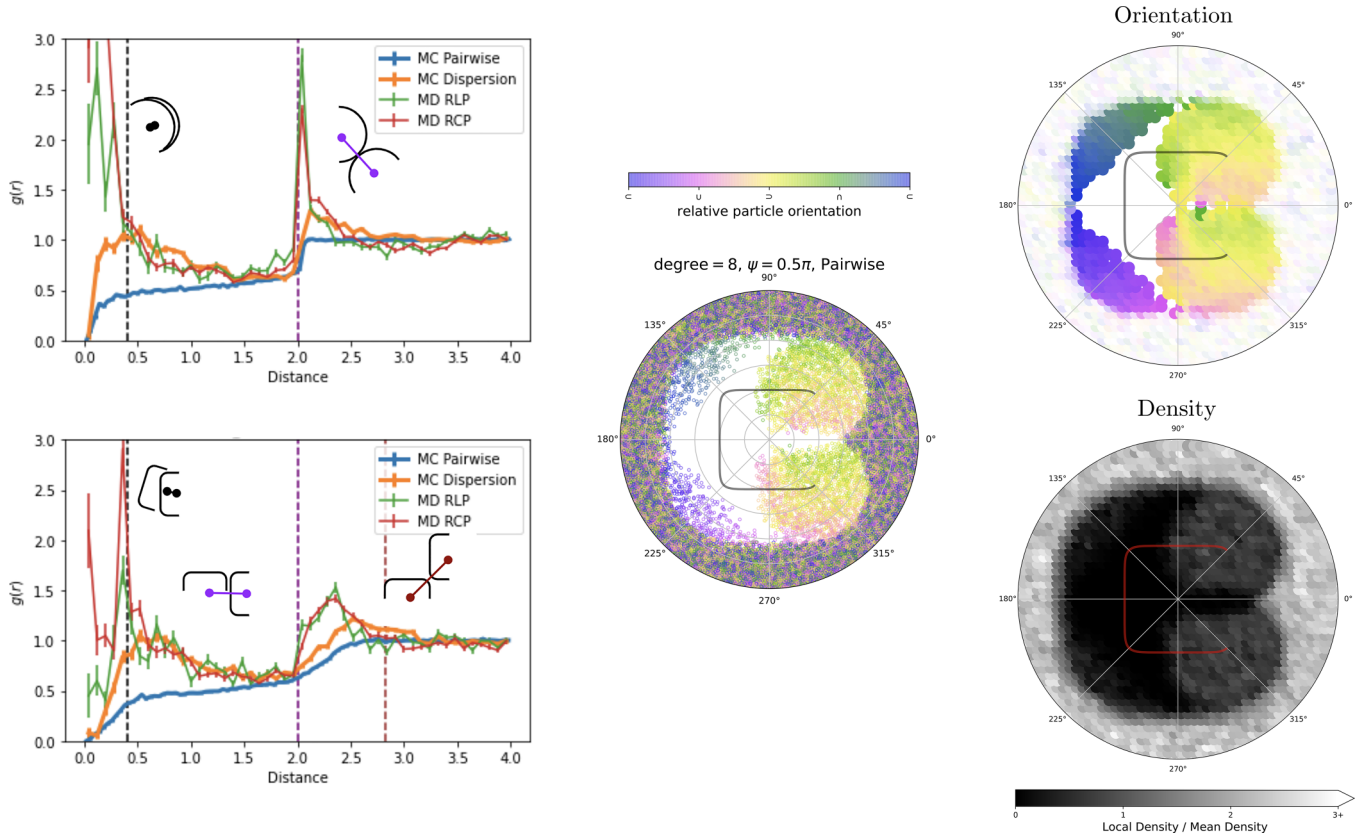


FIG. 4. Left: Pair correlation function  $g(r)$  for semicircular (top) and staple-shaped (bottom) SeSPs. The distributions show a step at (semicircles) or slightly beyond (U shaped)  $r = 2$ , the distance at which particles can always be placed regardless of orientation. Peaks around these values are seen in both dispersions and packings, indicating preferential locations for more densely packed particles and identifying a characteristic length scale for the collections. Middle/right: Three methods of visualizing the positions and orientations of particles relative to a central sample particle. Middle: a SODA plot, in which each point represents the center of a nearby SeSP, and the color indicates relative orientation. Upper Right: an orientation map, in which pixel hue corresponds to the average orientation of nearby particles within a certain distance of that pixel, and pixel saturation indicates the standard deviation of those orientations. Full saturation corresponds to a standard deviation of zero, and zero saturation corresponds to a standard deviation equal to or greater than the standard deviation of a uniform distribution. Lower Right: a density map, in which pixel lightness corresponds to the number of nearby particle centers within a certain distance of that pixel, normalized by the mean number of nearby particles.

between particles. Significant deviations from this prediction imply a substantially correlated packing with local ordering in either position, orientation, or both.

We calculate the particle excluded area for each shape from pairwise simulations as in [23]. This process numerically (and repeatedly) places two particles at random in an enclosed space  $A_{\text{box}}$  and counts the fraction of placements that result in an overlap between the two particles,  $N_{\text{overlap}}/N_{\text{tot}}$ , where  $N_{\text{tot}}$  is the total number of attempts. The excluded area is then the enclosed area multiplied by this fraction,  $A_{\text{box}} \times N_{\text{overlap}}/N_{\text{tot}}$ . We identify the mean coordination number at every step of each molecular dynamics simulation by counting contacts. Figure 3 plots the mean coordination number minus the value predicted by the mean contact model against that prediction, with zero deviation from the model prediction indicated by dashed black lines. Figure 3 shows good agreement between simulation and model for low packing fractions, where contacts between particles are relatively sparse, but divergence for many SeSP shapes even well below RLP (indicated by circular markers on the plot), with the disagreement growing

as the packing density increases. The agreement varies significantly based on particle shape; higher-opening-angle SeSPs tend to have fewer contacts at a given packing fraction than the model would predict, with a larger deviation for larger opening angles. This tendency does not appear to hold for order-1/2 SeSPs, which remain highly angular even at large opening angles.

The monotonic growth in the deviation of the system from the behavior predicted by the random contact model is a plausible consequence of the packing preparation and suggests that random loose packings form with fewer rearrangements driven by particle-particle interactions than random close packing, for which the packing process involves much more substantial rearrangement to enable the denser configuration. These rearrangements result in correlations between neighbors and therefore violate the random contact model's assumptions. The same effect was observed in quasi-two-dimensional, experimental packings of rods [1], a particle geometry equivalent to SeSPs of  $n \gg 2$  and  $\Psi > 3\pi/2$ . These results highlight the need to understand particle-scale

mechanics in order to understand the material's bulk structure and response.

### B. Spatial and spatioorientational correlations

The pair-correlation function

$$g(r) = \frac{A}{N^2} \frac{\sum_i n_i(r, r + dr)}{2\pi r dr} \quad (2)$$

measures the probability of finding another particle's center of curvature as a function of the distance  $r$  from another particle's center of curvature. The numeric calculation of  $g(r)$  is an ensemble average over all pairwise combinations of particles and is normalized to  $g(r \rightarrow \infty) = 1$ . Figure 4 (left) shows the resulting distribution for MC pairwise (blue) and dispersions (orange), and MD random loose (green) and close (red) packings of SeSPs with  $\Psi = \pi$  and  $n = 2$  (top) or  $n = 8$  (bottom) particles.

For SeSPs with opening angle  $\Psi = \pi$ , the particle shape and finite thickness prevents particles' centers-of-masses from overlapping, and so  $g(r \rightarrow 0) = 0$ . The pairwise data show a smooth, rapid rise from zero before a slowly increasing plateau for  $0.5 < r < 2$  (in units of particle radius of curvature). The plateau for pairwise particles arises because the number of nonoverlapping orientations does not appreciably increase as the particles move apart. This changes at  $r = 2$ , where all orientations are allowed, and the distribution jumps again to one. For  $r > 2$ , all orientations are allowed and  $g(r > 1) \equiv 1$ . The pairwise distribution represents the least dense configuration and a lower bound for dispersions and packings.

This is seen in the comparison with the resulting curve from dispersions. This curve rises from zero to a peak at  $r \approx 0.5$ , representing the increased probability of close nearest neighbors. The dashed line at  $r = 0.4$  corresponds to the spooning/nesting orientation shown in Fig. 4 (top left). As the dispersion is populated, these orientations are used to fit additional particles into the small spaces. This peak is still larger for MD packings at random loose and close packings, and is shifted slightly leftward to smaller values of  $r$  as a consequence of the rearrangements enforced by the packing procedure. During this process, particles will reorient very slightly to explore configurations with larger packing fractions, increasing the probability of finding neighbors at the nearest possible separations. In the corresponding plot for SeSPs with  $n = 8$ , Fig. 4 (bottom left), the peaks are shifted rightward toward larger  $r$  (compared with semi-circular particles), as the larger square diagonal further separates particles. The peaks in the packings for distributions again appear at slightly smaller separation distances as the packing protocol allows for optimization of packing.

The complex interaction between particle location and orientation was represented in Ref. [23] with spatioorientational distribution area or "SODA" plots [Fig. 4 (center right)] in which locations (dots) of particles relative to the (shown) reference particle are colored based on the relative orientation of the SeSPs. This representation allows one to identify four distinct regions. First, the space behind the reference particle is primarily comprised of particles oriented in the same direction (purples and blues) as the reference particle, creating a "spooning" or "nesting" region. Second, around each endpoint of the reference particle is a circular region of particles

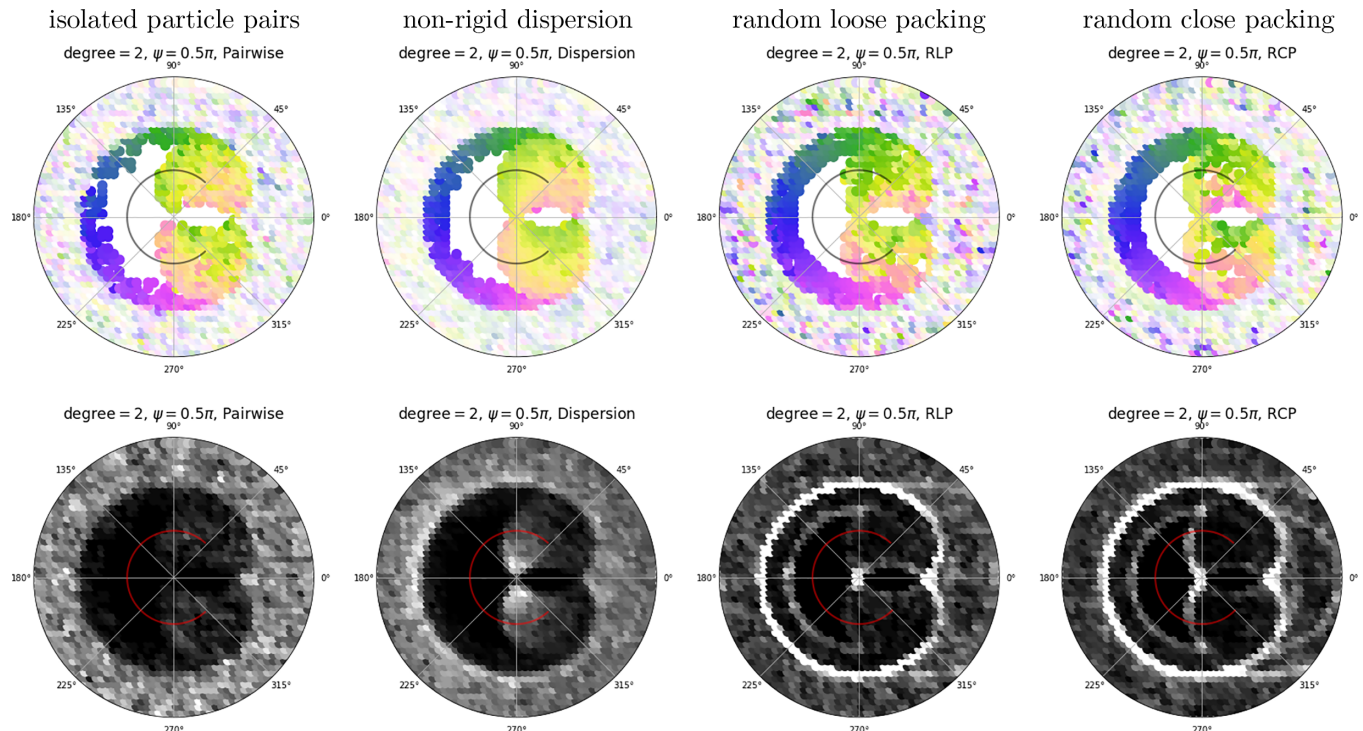


FIG. 5. SODA plots decomposed into orientation maps (top) and density maps (bottom) are shown for  $n = 2$ ,  $\Psi = \frac{\pi}{2}$  SeSPs generated (left to right, as indicated) as isolated particle pairs, as a nonrigid dispersion, at random loose packing, and at random close packing.

primarily in the opposing direction of the reference particle (light yellows, greens, and pinks), an entanglement region. Third, for  $\Psi < \pi$  a small white area where these two circular regions overlap indicates an excluded region where particles cannot be placed regardless of orientation. This excluded region also extends to a sizable area inside the nesting region where the opening is too small to permit nesting behavior. Finally, at the boundaries of each SODA plot, particles can be placed regardless of orientation, seen in the presence of dots of all colors.

The features described above capture the general traits of all SODA plots, whether generated for isolated particle pairs, nonrigid dispersions, or rigid packings and for varied SeSP parameters. The contrasts between these SODA plots offer a hint as to how local structure emerges as multiparticle interactions play an increasingly important role in constraining the availability of particular pairwise configurations. In order to disentangle orientational correlations and density correlations that emerge in the SODA plots, we can decompose a SODA plot into a locally averaged colormap of mean relative orientation, where the saturation of the colormap is inversely related to the standard deviation of the relative orientation, and a grayscale heatmap illustrating the probability of finding another SeSP centered at a particular point relative to the reference SeSP. An example of the decomposition is shown in Fig. 4 (right), and decomposed SODA plots for  $n = 2$ ,  $\Psi = \frac{\pi}{2}$  SeSPs for each of the isolated particle pairs (left), nonrigid dispersions (center-left), and rigid packings (RLP center right, RCP right) are shown in Fig. 5.

In the decomposed SODA plots, we observe that both density and orientational correlation tend to change abruptly at the boundaries between spooning, nesting, and noninteracting regions. In all of the systems analyzed, the orientational correlation drops off abruptly at the edges of the interacting regions and typically transitions sharply in a direction between the nesting region and the entangled region, indicating the sudden change in permitted angles. The behavior of the density at these boundaries varies between the different methods of producing the packings in the same way as  $g(r)$ ; the rigid packings feature sharp peaks in density along these boundaries due to particles rearranging to pack more tightly, while the nonrigid dispersions feature more gradual peaks and the isolated particle pairs simply drop off in density. The density maps for rigid packings also sometimes feature peaks in density outside of the interaction zones due to three-or-more particle interactions; for instance, the density plot for random close packing in Fig. 5 features peaks to the right of

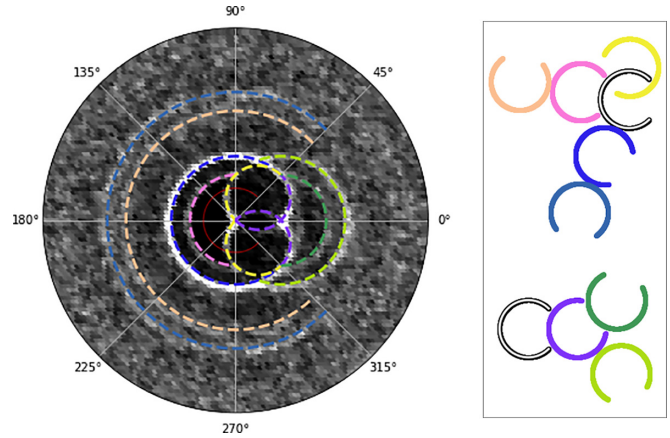


FIG. 6. (Left) Extended SODA density map for  $n = 2$ ,  $\Psi = \frac{\pi}{2}$  SeSPs, with regions of high density colored. (Right) Schematic representation of the first- and second-order contacts that generate these high-density regions, shown relative to two black reference SeSPs, with colors corresponding to the high-density region they represent.

the entanglement zones due to interactions with a SeSP in the opening of the reference SeSP, and a zoomed-out version of this density plot in Fig. 6 illustrates more distant peaks which relate to other types of three-particle interactions.

#### IV. CONCLUSION

We have explored the statistics of multiparticle configurations of superellipsoidal sector particles, a framework that can approximate an extraordinarily broad class of 2D particle shapes. We have measured the critical random (loose and close) packing fractions and their correlation to the calculated excluded area, finding discrepancies with the predictions of the mean-field random contact model. The deviation from the random contact model expectation grows monotonically with volume fraction, even well below random loose packing. These discrepancies are explained by the complex relationship between spatial proximity and orientational alignment, allowing particles to pack more densely through coordinated spatioorientational positioning with neighbors.

#### ACKNOWLEDGMENT

We acknowledge helpful input and discussion from the members of the Soft Matter Research Group at the RIT School of Physics and Astronomy, and from members of the Tri-College Soft Matter group.

- [1] K. Stokely, A. Diacou, and S. V. Franklin, Two-dimensional packing in prolate granular materials, *Phys. Rev. E* **67**, 051302 (2003).
- [2] Kenneth Desmond performed this work as a sophomore in 2004.
- [3] N. Gravish, S. V. Franklin, D. L. Hu, and D. I. Goldman, Entangled granular media, *Phys. Rev. Lett.* **108**, 208001 (2012).
- [4] S. V. Franklin, Extensional rheology of entangled granular materials, *Europhys. Lett.* **106**, 58004 (2014).
- [5] A. Donev, I. Cisse, D. Sachs, E. A. Variano, F. H. Stillinger, R. Connelly, S. Torquato, and P. M. Chaikin, Improving the density of jammed disordered packings using ellipsoids, *Science* **303**, 990 (2004).
- [6] H. M. Beakawi Al-Hashemi and O. S. Baghabra Al-Amoudi, A review on the angle of repose of granular materials, *Powder Technol.* **330**, 397 (2018).
- [7] M. Trepanier and S. V. Franklin, Column collapse of granular rods, *Phys. Rev. E* **82**, 011308 (2010).

- [8] N. Gravish and D. I. Goldman, *Entangled Granular Media*, chapter 17, pp. 341–354, John Wiley & Sons, Ltd, 2016.
- [9] Y. Zhao, J. Barés, and J. E. S. Socolar, Yielding, rigidity, and tensile stress in sheared columns of hexapod granules, *Phys. Rev. E* **101**, 062903 (2020).
- [10] N. Weiner, Y. Bhosale, M. Gazzola, and H. King, Mechanics of randomly packed filaments—the “bird nest” as meta-material, *J. Appl. Phys.* **127**, 050902 (2020).
- [11] K. A. Murphy, A. K. MacKeith, L. K. Roth, and H. M. Jaeger, The intertwined roles of particle shape and surface roughness in controlling the shear strength of a granular material, *Granular Matter* **21**, 72 (2019).
- [12] D. Wang, H. Zheng, Y. Ji, J. Barés, and R. P. Behringer, Shear of granular materials composed of ellipses, *Granular Matter* **22**, 5 (2020).
- [13] D. Dumont, M. Houze, P. Rambach, T. Salez, S. Patinet, and P. Damman, Emergent strain stiffening in interlocked granular chains, *Phys. Rev. Lett.* **120**, 088001 (2018).
- [14] Y. Yang, H. Pei, G. Chen, K. T. Webb, L. J. Martinez-Miranda, I. K. Lloyd, Z. Lu, K. Liu, and Z. Nie, Phase behaviors of colloidal analogs of bent-core liquid crystals, *Sci. Adv.* **4**, eaas8829 (2018).
- [15] E. R. Chen, D. Klotsa, M. Engel, P. F. Damasceno, and S. C. Glotzer, Complexity in surfaces of densest packings for families of polyhedra, *Phys. Rev. X* **4**, 011024 (2014).
- [16] C. Fernández-Rico, M. Chiappini, T. Yanagishima, H. de Sousa, D. G. A. L. Aarts, M. Dijkstra, and R. P. A. Dullens, Shaping colloidal bananas to reveal biaxial, splay-bend nematic, and smectic phases, *Science* **369**, 950 (2020).
- [17] A. Jáklí, O. D. Lavrentovich, and J. V. Selinger, Physics of liquid crystals of bent-shaped molecules, *Rev. Mod. Phys.* **90**, 045004 (2018).
- [18] W. D. Hodson and T. G. Mason, Lock-and-key dimerization in dense brownian systems of hard annular sector particles, *Phys. Rev. E* **94**, 022124 (2016).
- [19] P.-Y. Wang and T. G. Mason, Colloidal lock-and-key dimerization reactions of hard annular sector particles controlled by osmotic pressure, *J. Am. Chem. Soc.* **137**, 15308 (2015).
- [20] Y. Geng, G. van Anders, P. M. Dodd, J. Dshemuchadse, and S. C. Glotzer, Engineering entropy for the inverse design of colloidal crystals from hard shapes, *Sci. Adv.* **5**, eaaw0514 (2019).
- [21] S. C. Glotzer and M. J. Solomon, Anisotropy of building blocks and their assembly into complex structures, *Nat. Mater.* **6**, 557 (2007).
- [22] J. P. Ramírez González and G. Cinacchi, Dense packings of hard circular arcs, *Phys. Rev. E* **102**, 042903 (2020).
- [23] K. Kornick, T. Brzinski, and S. V. Franklin, Excluded area of superellipse sector particles, *Phys. Rev. E* **104**, 034904 (2021).
- [24] G. Lu, R. C. Hidalgo, J. R. Third, and C. R. Müller, Ordering and stress transmission in packings of straight and curved spherocylinders, *Granular Matter* **18**, 34 (2016).
- [25] A. P. Thompson, H. M. Aktulga, R. Berger, D. S. Bolintineanu, W. M. Brown, P. S. Crozier, P. J. in ’t Veld, A. Kohlmeyer, S. G. Moore, T. D. Nguyen, R. Shan, M. J. Stevens, J. Tranchida, C. Trott, and S. J. Plimpton, LAMMPS - a flexible simulation tool for particle-based materials modeling at the atomic, meso, and continuum scales, *Comput. Phys. Commun.* **271**, 108171 (2022).
- [26] D. J. Jacobs and B. Hendrickson, An algorithm for two-dimensional rigidity percolation: The pebble game, *J. Comput. Phys.* **137**, 346 (1997).
- [27] J. Clerk Maxwell F. R. S., Xlv. on reciprocal figures and diagrams of forces, *Lond. Edinb. Dublin philos. mag. j. sci.* **27**, 250 (1864).
- [28] K. Liu, J. E. Kollmer, K. E. Daniels, J. M. Schwarz, and S. Henkes, Spongelike rigid structures in frictional granular packings, *Phys. Rev. Lett.* **126**, 088002 (2021).
- [29] D. J. Jacobs and M. F. Thorpe, Generic rigidity percolation in two dimensions, *Phys. Rev. E* **53**, 3682 (1996).
- [30] W. G. Ellenbroek, V. F. Hagh, A. Kumar, M. F. Thorpe, and M. van Hecke, Rigidity loss in disordered systems: Three scenarios, *Phys. Rev. Lett.* **114**, 135501 (2015).
- [31] S. Henkes, D. A. Quint, Y. Fily, and J. M. Schwarz, Rigid cluster decomposition reveals criticality in frictional jamming, *Phys. Rev. Lett.* **116**, 028301 (2016).
- [32] D. J. Koeze and B. P. Tighe, Sticky matters: Jamming and rigid cluster statistics with attractive particle interactions, *Phys. Rev. Lett.* **121**, 188002 (2018).
- [33] S. Zhang, L. Zhang, M. Bouzid, D. Zeb Rocklin, E. Del Gado, and X. Mao, Correlated rigidity percolation and colloidal gels, *Phys. Rev. Lett.* **123**, 058001 (2019).
- [34] K. Liu, S. Henkes, and J. M. Schwarz, Frictional rigidity percolation: A new universality class and its superuniversal connections through minimal rigidity proliferation, *Phys. Rev. X* **9**, 021006 (2019).
- [35] H. A. Vinutha and S. Sastry, Force networks and jamming in shear-deformed sphere packings, *Phys. Rev. E* **99**, 012123 (2019).
- [36] A. P. Philipse, The random contact equation and its implications for (colloidal) rods in packings, suspensions, and anisotropic powders, *Langmuir* **12**, 1127 (1996).